Scientific Contributions Oil & Gas, Vol. 49. No. 1, March: 105 - 123

SCIENTIFIC CONTRIBUTIONS OIL AND GAS

Testing Center for Oil and Gas
LEMIGAS

Journal Homepage:http://www.journal.lemigas.esdm.go.id
ISSN: 2089-3361, e-ISSN: 2541-0520

Reservoir Characterization of the Terumbu and Arang Formations Using Model-Based Seismic Inversion in the East Natuna Basin

Guntur Adham Syah Putra[1], Abdul Haris[1], Ricky Adi Wibowo[1], and Edy Wijanarko [2]

[1]Department of Physics, FMIPA University of Indonesia
Lingkar Street, Pondok Cina, Beji Sub-district, Depok City, West , Indonesia.

[2]Testing Center for Oil and Gas LEMIGAS
Ciledug Raya Street Kaveling 109, Cipulir, Kebayoran Lama, South Jakarta, Indonesia.

Corresponding author: Guntur Adham Syah Putra (gunturadham@gmail.com)

Manuscript received: January 05th, 2026; Revised: January 28th, 2026
Approved: January 30th, 2026; Available online: March 06th, 2026; Published: March 09th, 2026.

ABSTRACT - The Miocene carbonate buildup and fine-grained clastic sequence constitute the main reservoir and sealing intervals in the East Natuna Basin. This study characterizes the reservoirs of the Terumbu and Arang Formations using an integrated workflow that includes petrophysical analysis, sensitivity analysis, depth structure mapping, and model-based seismic inversion. Well-log interpretation shows clear lithological contrasts between the two formations. The Terumbu carbonates exhibit very low gamma-ray values (18 to 24 API) and high porosity, ranging from 28 to 37%, with neutron–density crossovers indicating gas-bearing intervals, particularly in the GADO-3 well, where resistivity values range from 852 to 1958 Ω·m. In contrast, the Arang Formation is characterized by high gamma-ray values (102 to 148 API), higher clay volume (30 to 44%), and low porosity (<10%). P-impedance–density cross-plots distinguish carbonate rocks (4,500 to 10,000 g/cc·m/s; 1.7 to 2.35 g/cc) from shale and shaly sand with higher impedance and density. Depth structure mapping reveals a central–northern structural high that is favorable for reef development and fault-related trapping. Model-based seismic inversion further reveals low-to-moderate impedance (4,100 to 6,156 g/cc·m/s), low density, and high inverted porosity within the Top Terumbu interval, indicating excellent reservoir quality. Overall, the results indicate that the Terumbu Formation forms the primary carbonate reservoir, while the Arang Formation mainly acts as an effective regional seal in the petroleum system of the East Natuna Basin.

Keywords: Reservoir characterization, acoustic impedance, model-based inversion, carbonate reservoir, east natuna basin, terumbu formation, arang formation.

Copyright © 2026 by Authors, Published by LEMIGAS

How to cite this article:

Guntur Adham Syah Putra, Abdul Haris, Ricky Adi Wibowo, and Edy Wijanarko, 2026, Terumbu and Arang Formation Characterization by Using Model Based Seismic Inversion in The East Natuna Basin, Scientific Contributions Oil and Gas, 49 (1) pp. 105-213. DOI org/10.29017/scog.v49i1.1979.

INTRODUCTION

Indonesia has significant petroleum potential in 128 sedimentary basins by only ~15.6% being explored and exploited by oil and gas companies (Kementerian Energi dan Sumber Daya Mineral 2022). This presents a considerable potential to find new hydrocarbons, especially in unexplored and frontier basins. Another case where a lot is written, but not integrated, is the Natuna basin in the southern South China Sea. The area is divided approximately in half among the West and East Natuna areas that are themselves split by the Natuna Arch a structural high made up of Jurassic Cretaceous metamorphic rocks (Darman 2017).

The East Natuna Basin is considered as a discovery basin considering the existence of hydrocarbons that was confirmed, that mostly gas in giant Natuna D-Alpha field found in 1973 by more than 200 TCF (Trillium Cubic Feet) sized gas and high CO_2 content (71%) (Darman 2017). Exploration effort in the East Natuna Basin is significantly lower than that of the West Natuna Basin despite numerous proven plays syn-rift graben systems, post-rift clastics and extensive Miocene carbonate buildups (Darman, 2017). Several recent exploration wells including Kuda Laut-1 and Singa Laut-1, drilled by Premier Oil in 2014 demonstrate the presence of Oligocene syn-rift reservoirs, reinforcing the basin's exploration significance.

Stratigraphically, the East Natuna Basin shares similarities by the West Natuna Basin and the Sarawak Luconia carbonate province. The package in the sedimentary cover is composed by a base-up, by the upper part of ipper gabus formation (upper syn-rift clastics paleogene), arang formation (lower -middle miocene source rock and shale-dominated interval), terumbu formation (well-developed Miocene carbonates platform) and Muda Formations (Younger clastics) (Darman, 2017).The Arang Formation acts as both a regional source rock and a sealing unit, while it comprises the reservoir intervals including Arang Sand intercalated by Arang Shale. At the same time, the Terumbu Formation forms widespread carbonate platforms by reefal facies that also have significant reservoir potential as is proven by the Natuna D-Alpha discovery.

Despite a wide geographical distribution of the region, well documented reservoir characterization through Terumbu and Arang formations is scarce. Due to complex geological structure of the East Natuna Basin; syn-rift fault blocks, graben systems such as Komodo and Sokang Grabens, and huge carbonate buildups required a comprehensive geophysical and petrophysical investigation in order to decrease the exploration risk (Darman 2017).

Seismic inversion based on modeling has been recognized as one of the most effective approaches for identifying lithology and fluid distribution. Acoustic impedance (AI) volumes are generated by seismic amplitude data, allowing the detection of carbonate formations, sand shale sequences, and zones by potential hydrocarbon presence to be improved (Veeken 2007). AI is especially useful for differentiating reefal carbonates in the Terumbu Formation by the contrasting lithologies of Arang Sand and Arang Shale. Complementary seismic attributes—particularly amplitude and frequency help identify anomalies associated by the presence of hydrocarbons, structural traps, and stratigraphic variations (Darman 2017). Petrophysical analysis further refines reservoir parameters, including porosity and permeability, and saturation, improving confidence in subsurface interpretation.

The primary objective of this study is set to characterize the reservoir intervals of the Terumbu and Arang Formations, by emphasis placed on the identification of reefal carbonate facies, Arang Sand, and Arang Shale. Lithological distribution is intended to be delineated, reservoir quality assessed, and hydrocarbon potential evaluated in the East Natuna Basin through the integration of model-based seismic inversion and petrophysical analysis. The outcomes are anticipated to provide guidance for future exploration strategies and to support ongoing efforts aimed at discovering new plays inside of Indonesia's underexplored basins.

METHODOLOGY

Table 1. Seismic data

Seismic Data	Sample Rate (ms)
Line 01	4
Line 02	4
Line 04	4
Line 05	4
Line 06	4
Line 07	4
Line 08	4
Line 20	4
Line 21	4
Line 23	4

This research utilizes 2D post-stack time-migrated seismic data in combination by four well logs. These seismic and well-log datasets, that form the basis of the analysis, are summarized in Table 1 and Table 2.

Acoustic impedance

Acoustic impedance is considered a physical parameter that quantifies the resistance of a medium to the propagation of acoustic waves. It is defined mathematically as the product of the density (ρ) and the velocity (v) of the acoustic wave traveling through the medium. The relationship is expressed by the following equation:

$$AI = \rho \times v \quad (1)$$

Acoustic impedance values are affected by lithology, porosity, fluid content, depth, and pressure. Consequently, it can be utilized as an indicator for lithology differentiation, porosity evaluation, and quantitative reservoir characterization (Russell 1988).

Reflection coefficient

The reflection coefficient is defined as a parameter that measures the proportion of seismic wave energy that is reflected when a boundary among two rock layers by differing acoustic impedance values is encountered.

Table 2. Well log data

Log Data	GAAX-1	GAAN-2	GADO-3	GANG-4
GR	√	√	√	√
CALIPER	√	√	√	√
SP	√	√	√	√
MSFL	-	√	√	√
RESL	-	√	-	√
RESM	√	√	√	√
RESD	√	√	√	√
NPHI	-	√	√	√
RHOB	-	√	√	√
DT	√	√	√	√
CORE POROSITY	√	√	-	-
CORE PERMEABILTY	√	√	-	-

The reflection coefficient (KR) obtained by measurements is calculated using the following equation:

$$R = \frac{AI_2 - AI_1}{AI_2 + AI_1} \quad (2)$$

Model based inversion

Model-based inversion (MBI) is a post-stack inversion technique commonly used to derive acoustic impedance (AI) by seismic reflection data. The method relies on the one-dimensional convolutional model, in that a seismic trace is expressed as the convolution among a seismic wavelet and the subsurface reflectivity function, by the addition of noise by acquisition instruments or cultural sources. This fundamental relationship is expressed as:

$$S(t) = W(t) * R(t) + N(t) \quad (3)$$

As long as the noise component does not correlate by the true seismic signal, the subsurface reflectivity can still be reliably estimated. (Russell, 1988) developed a nonlinear iterative formulation that enables the progressive calculation of acoustic impedance by reflectivity. Through recursive inversion, this approach converts reflection coefficients into an acoustic impedance model. In this formulation, Z_1represents the AI of the first (uppermost) layer, Z_Nis the AI of the N-th layer, and r_idenotes the reflection coefficient at the boundary of the i-th layer.

In practice, MBI is implemented using the Generalized Linear Inversion (GLI) method to generate the impedance model that best fits the observed seismic data. According to Russell (1988), the seismic forward modeling function can be linearized to relate the seismic response to the earth model as follows:

$$F(M) \approx F(M_0) + G\Delta M \quad (4)$$

where M_0is the initial impedance model, Gis the sensitivity (derivative) matrix, and ΔMis the model update. The correction to the model parameters is obtained using the least-squares solution:

$$\Delta M = (G^T G)^{-1} G^T \Delta F \quad (5)$$

The inversion is designed to minimize an objective function that considers both the discrepancy among recorded and synthetic seismic traces and the difference among the actual and calculated acoustic impedance:

$$J = W_1(S_r - S_c)^2 + W_2(AI_r - AI_c)^2 \quad (6)$$

Iterative minimization of this objective function produces a final impedance model that more accurately reflects subsurface lithology and reservoir properties.

The reflection coefficient is a parameter that indicates the proportion of seismic wave energy reflected when the wave encounters a boundary among two rock layers by different acoustic impedance values.

The methodological workflow applied in this research comprises several integrated stages. The study begins by data preparation, using 2D post-stack seismic data, four well logs, and regional geological information, all of that undergo quality control prior to processing. Well log analysis is then performed to determine lithology, fluid type, and porosity, and other petrophysical parameters, supported by cross-plotting to evaluate relationships among acoustic impedance, density, sonic velocity, porosity, and gamma-ray values. A statistical wavelet is extracted by the seismic dataset, followed by a well-to-seismic tie to ensure accurate correlation and phase alignment among well-log signatures and seismic reflections in the time domain. Key horizons and stratigraphic markers are interpreted based on well data. Using these inputs, an initial acoustic impedance model is constructed and subsequently refined through model-based inversion (MBI) using the GLI method, following the iterative approaches of Russell (1988), until the synthetic and observed seismic traces achieve an optimal match. Porosity is then estimated by applying a linear AI porosity

relationship, derived by well-log cross-plots, to the inverted AI model. Finally, lithology and fluid content are interpreted using the outcome acoustic impedance and porosity volumes, This process leads to the evaluation of reservoir characteristics inside of the Terumbu and Arang Formations.

RESULT AND DISCUSSION

Petrophysical interpretation and analysis

Well log data represent one of the most sensitive subsurface datasets for detecting variations in lithology and fluid content, making them essential for delineating potential reservoir intervals. Target interval identification in this study was carried out through a quick-look interpretation by examining the individual responses of each log curve, by evaluated intervals in wells GAAX-1, GAAN-2, GADO-3, and GANG-4 highlighted in Figures 1 4. The initial interpretation incorporated Gamma Ray (GR), resistivity, and porosity logs (NPHI and RHOB), that collectively provide complementary insights for distinguishing lithology, reservoir quality, and pore-fluid conditions (Rider, 1996). GR analysis provides the primary lithological indicator, as high natural radioactivity typically corresponds to shale due to its elevated clay mineral content, whereas clean sandstones and carbonates generally yield lower GR responses (Rider, 1996). In Well GADO-3, The Terumbu interval (1,898 3,158 ft) exhibits low GR values of 18 21 API, consistent by clean limestone, supported by high porosity (0.28) and low clay volume (0.06). In contrast, the Arang interval (3158 9482 ft) shows much higher GR values (102 148 API), reflecting a progression by shaly sand in the shallower zone where moderate GR is accompanied by relatively high porosity and ~0.30 Vcl toward compact shale at greater depths where porosity significantly decreases. Well GAAX-1 exhibits a similarly diagnostic GR response: the Terumbu interval (3947 5528 ft) shows moderate GR values (~55 API) interpreted as shaly limestone by preserved porosity (0.37) and moderate clay content (0.37), Meanwhile, the overlying Arang interval (5,528 5,719 ft) displays higher GR values (63 API) and a clay volume of 0.44, characteristic of shaly sandstone or shale sand interbeds typical of clastic sequences inside of the Arang Formation. In Well GAAN-2, the Terumbu interval (3887 9589 ft) yields very low GR (24 API), This indicates clean limestone, despite relatively low porosity (0.12) outcome by compaction and diagenesis. The overlying Arang interval (9589 9747 ft) presents GR values around 48 API by high clay volume (0.40) and negligible porosity (0.2), reflecting compact shale. Meanwhile, Well GANG-4 exhibits exceptionally low GR values (18 API) and a low clay volume (0.15), and high porosity (0.31) inside of the Terumbu interval (2493 3400 ft), confirming a clean and high-quality carbonate reservoir.

Resistivity logs (MSFL for the flushed zone, RESM for the transition zone, and RESD for the uninvaded zone) are crucial for distinguishing conductive, brine-filled formations by hydrocarbon -bearing intervals (Ellis & Singer, 2007). In Well GADO-3, the resistivity curves exhibit a strong invasion profile, where the shallow resistivity (LLM) remains consistently low, at approximately ~3 Ù·m, while the deep resistivity (LLD) increases dramatically at multiple depths—reaching 1997 Ù·m at 6297 6317 ft, 852 Ù·m at 6706 6714 ft, 1042 Ù·m at 6808 6831 ft, and 1958 Ù·m at 6908 6941 ft. This pronounced contrast among LLD and LLM is a classic indicator of hydrocarbon-bearing zones (Asquith & Krygowski, 2004). In contrast, Well GAAX-1 does not contain resistivity data, while Well GAAN-2 shows uniformly low resistivity values (MSFL 5 Ù·m, RESM 3 Ù·m, RESD 4 Ù·m), This reflects brine-filled intervals in both the Terumbu and Arang formations, consistent by interpretations of low-porosity limestone and conductive shale. Similarly, Well GANG-4 generally displays low resistivity (MSFL 4 Ù·m, LLS 2.5 Ù·m, LLD 2 Ù·m), except for a notable high-resistivity interval among 2456 2589 ft, that averages approximately 100 Ù·m and is interpreted as a potential carbonate prospect.

Porosity analysis based on neutron (NPHI) and density (RHOB) logs provides additional discrimination of fluid types. NPHI responds primarily to hydrogen-bearing fluids, while RHOB reflects rock density; Thus, a pronounced neutron density crossover, where RHOB falls below NPHI, is widely recognized as a signature of gas-filled

porosity due to gas's low hydrogen content and low density (Asquith & Krygowski 2004). In Well GADO-3, strong and consistent crossovers in the 6808 6831 ft and 6908 6941 ft intervals confirm gas-filled porosity. Well GAAX-1 lacks neutron density logs, whereas Well GAAN-2 exhibits only narrow or weak crossovers, consistent by brine-filled formations. In Well GANG-4, the Terumbu interval (2500 2569 ft) displays a wide and distinct neutron density crossover, by NPHI significantly lower than RHOB. This pronounced separation, combined by high porosity (~0.31), is a classic diagnostic of gas-bearing carbonate reservoirs in petrophysical interpretation. Furthermore, the absence of washout artifacts reinforces that this anomaly reflects genuine formation gas rather than borehole conditions.

Sensitivity analysis

The sensitivity analysis was conducted using a cross-plot of P-impedance versus density (RHOB), by gamma ray used as the color-coding parameter. The analysis is intended to assess the capability of each petrophysical log parameter in distinguishing the target lithologies, specifically carbonate rocks (limestone/reef) and fine-grained clastic rocks (shaly sand and shale) inside of the Terumbu and Arang formations. The outcomes obtained by the P -Impedance versus Density (RHOB) cross-plots for both wells are presented in Figures 5 and 6. The cross-plot for Well GADO-3 displays two major data clusters, representing significant lithological differences.

The first cluster is characterized by low medium density values (±1.7 2.45 g/cc) and low gamma ray readings. This cluster represents carbonate lithologies, particularly limestone and reefal carbonates. This density range is consistent by porous carbonate densities, where limestone typically ranges by 2.20 2.70 g/cc but may decrease in highly porous or altered intervals (Asquith & Krygowski 2004). The corresponding P-impedance values, ranging by 4,500 to 9,000 g/cc·m/s, reflect variations in porosity and possible fluid effects inside of the carbonate interval.

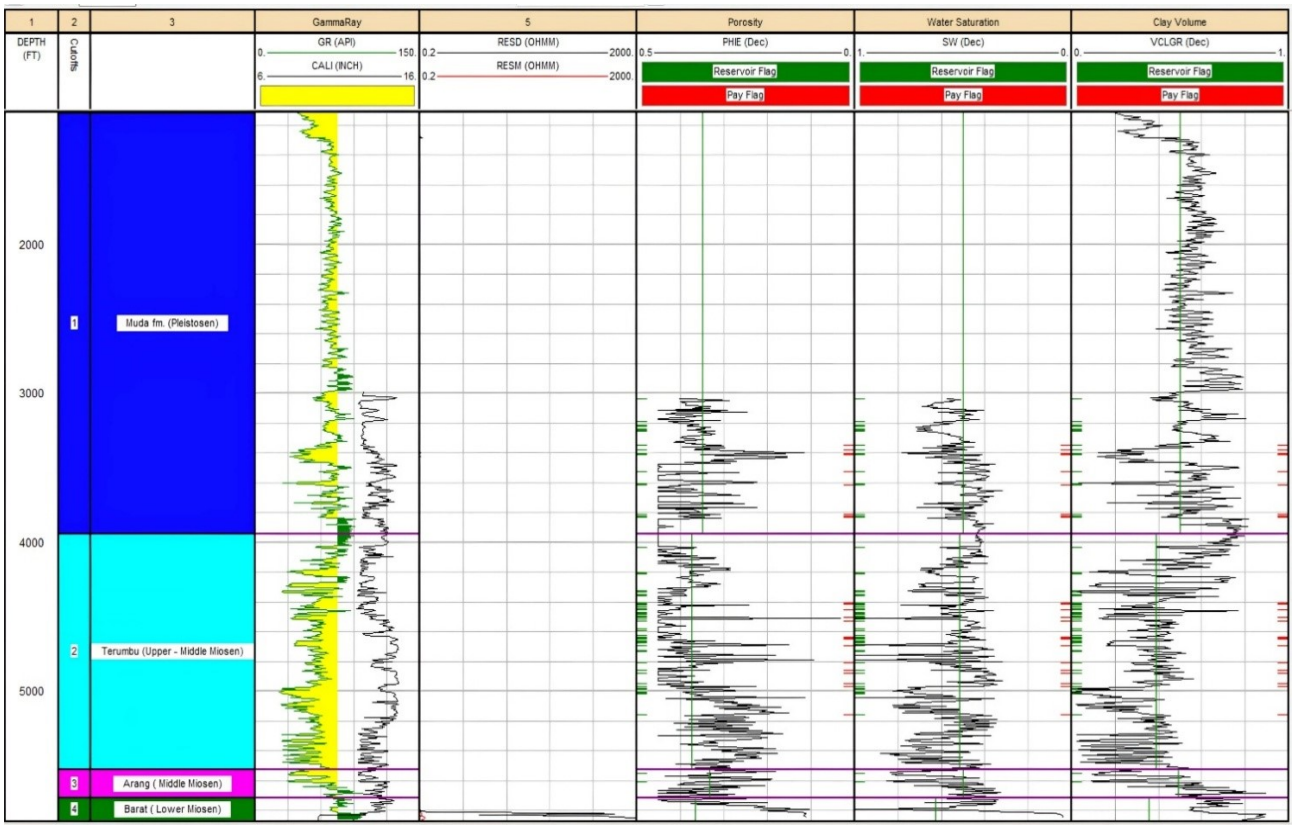

Figure 1. Log data of the GAAX-1 well in the Terumbu & Arang formation of the East Natuna Basin

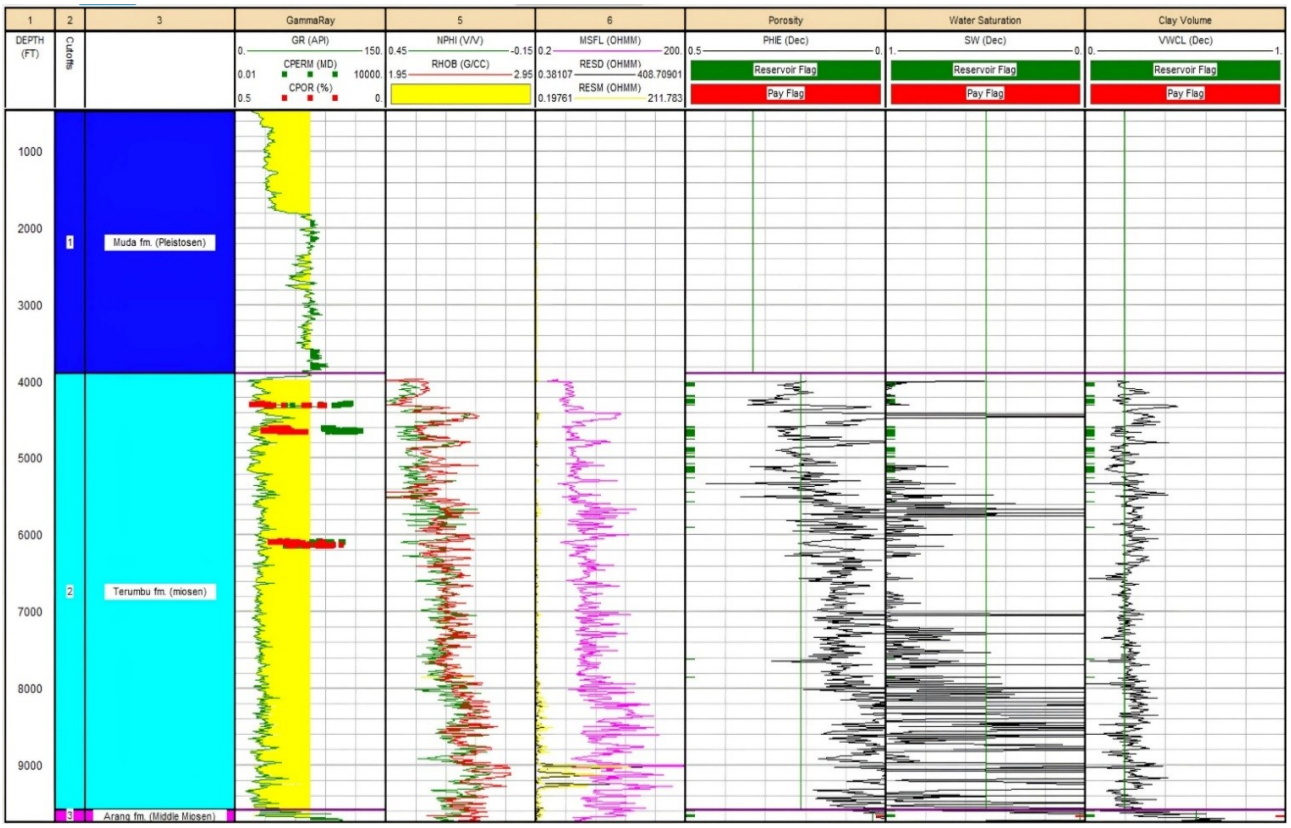

Figure 2. Log data of the GAAN-2 well in the Terumbu & Arang formation of the East Natuna Basin

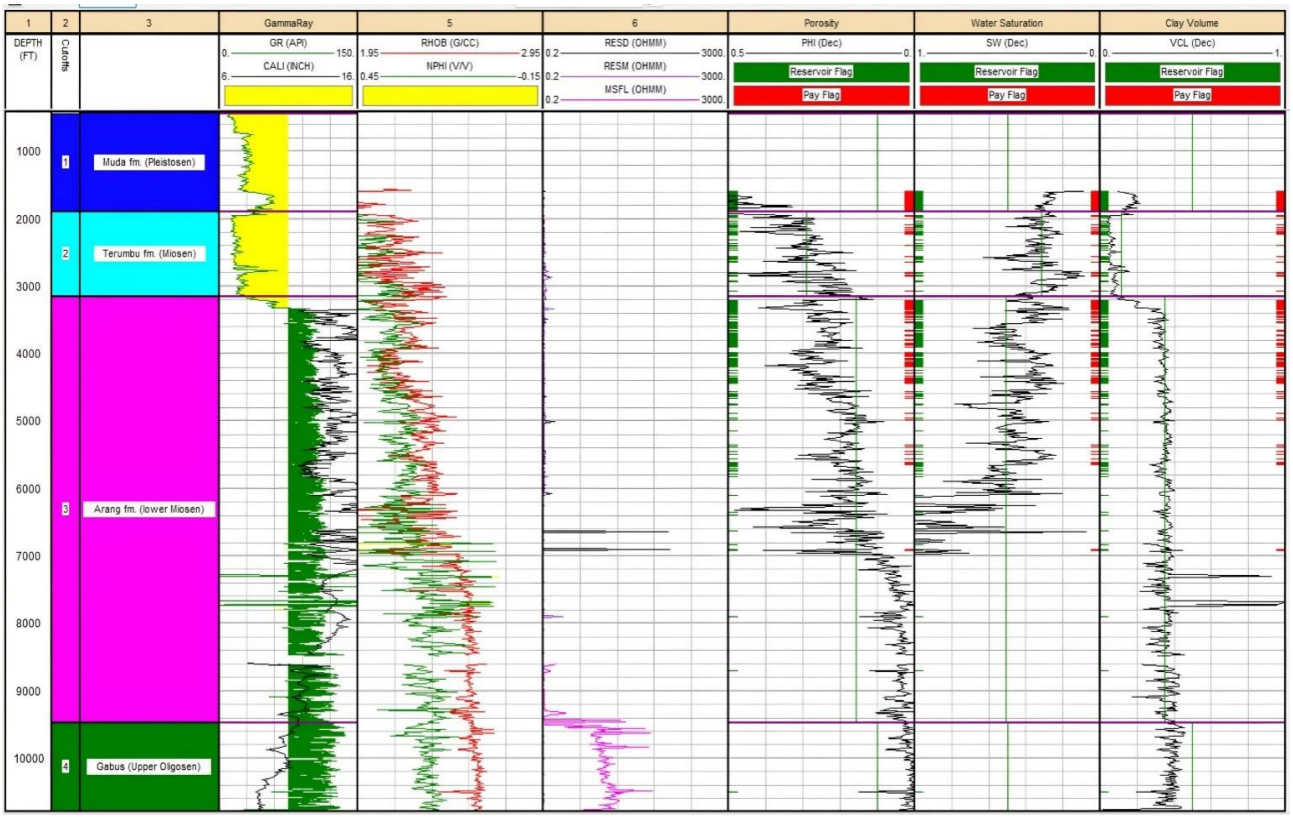

Figure 3. Log data of the GADO-3 well in the Terumbu & Arang formation of the East Natuna Basin

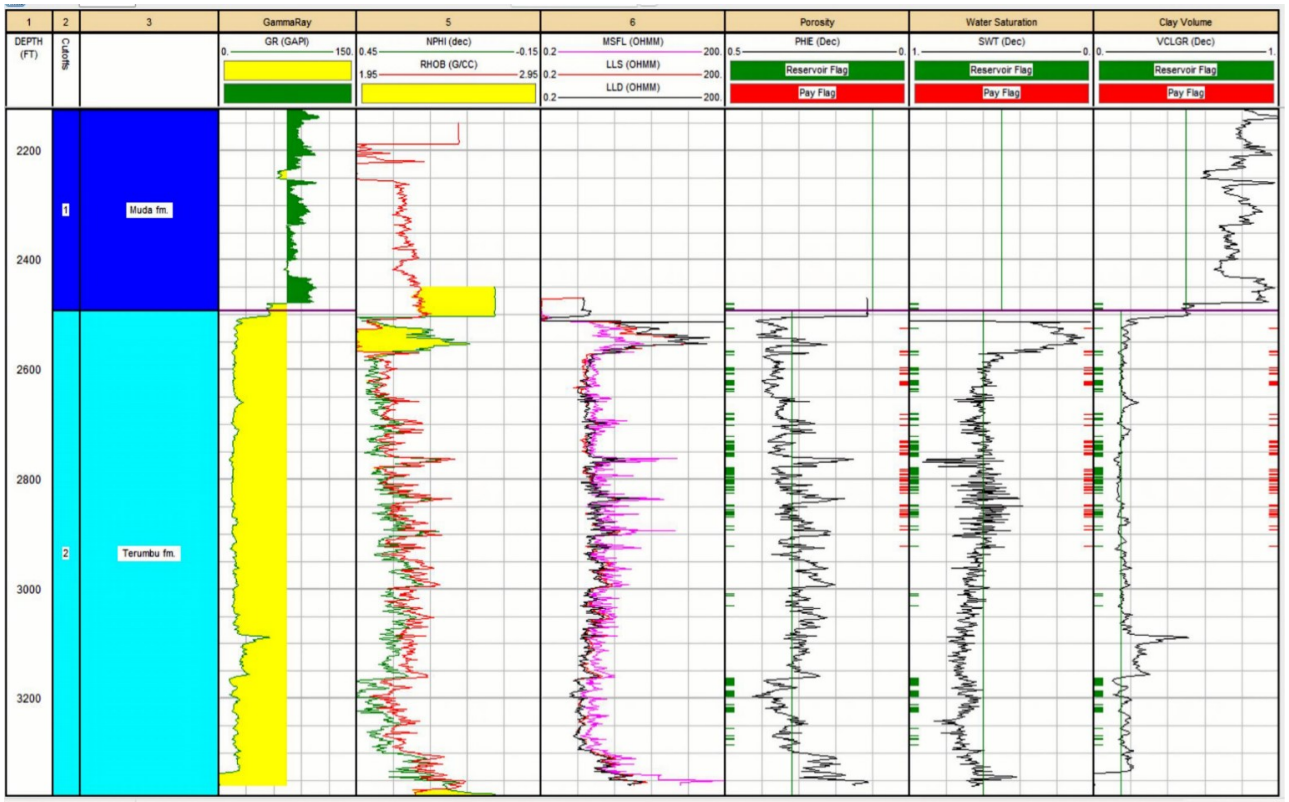

Figure 4. Log data of the GANG-4 well in the Terumbu formation of the East Natuna Basin

The second cluster is characterized by high gamma ray values (>150 gAPI) and higher densities (2.45 2.65 g/cc), combined by P-impedance values among 8000 13,000 g/cc·m/s. This pattern indicates shale or shaly sand lithologies, consistent by typical shale density ranges (2.40 2.70 g/cc) and sandy shale densities among 2.20 2.55 g/cc (Ellis & Singer 2007). The increase in gamma ray and density reflects finer-grained, compacted, clay-rich lithologies commonly associated by the Arang Formation.

Overlap among the two clusters occurs inside of the P-impedance range of 6000 9800000 g/cc·m/s, suggesting that impedance is influenced not only by lithology but also by variations in porosity, fluid saturation, and changes in P-wave velocity affected by fluid incompressibility (Rose et al., 2025).

A similar pattern is observed in Well GAAN-2, although the data distribution is more compact and clearly defined. The carbonate cluster is observed inside of the low to medium density range (approximately 1.90 2.35 g/cc) and low to medium GR values, by P-impedance values ranging by 6000 to 10,000 g/cc·m/s. This density range is considered indicative of porous limestone or reefal carbonate, that may display reduced densities due to high porosity or the presence of fractures (Asquith & Krygowski 2004; Schlumberger 1989).

The second cluster, exhibiting higher densities (2.35 2.65 g/cc), elevated GR values, and P-impedance values ranging by 9000 to 14,000 g/cc·m/s, is associated by shaly sand lithologies. The third cluster, defined by higher densities (2.35 2.80 g/cc), increased gamma ray values, and P-impedance values among 14,000 and 17,500 g/cc·m/s, is attributed to shale lithologies. These characteristics are observed to correspond by the typical density and gamma ray values of fine-grained clastic rocks inside of the Arang Formation (Ellis & Singer 2007). The increase in density and impedance reflects enhanced compaction and clay content.

Some data points are observed to overlap inside of the moderate impedance range (8,000 10,000 g/cc·m/s), potentially outcome by fluid effects, variations in the matrix, or heterogeneous porosity.

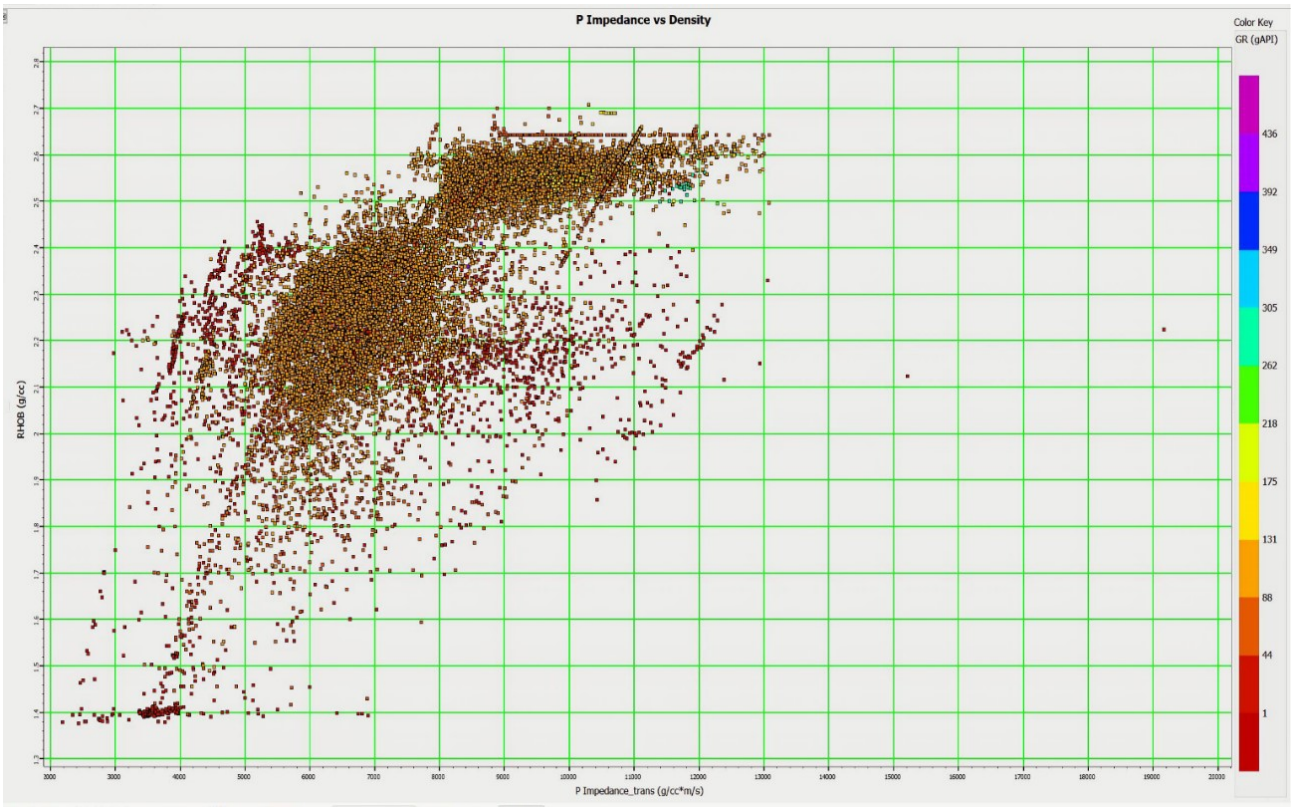

Figure 5. Cross-plot of P-impedance and density with color bar of gamma ray values in the GADO-3 wells

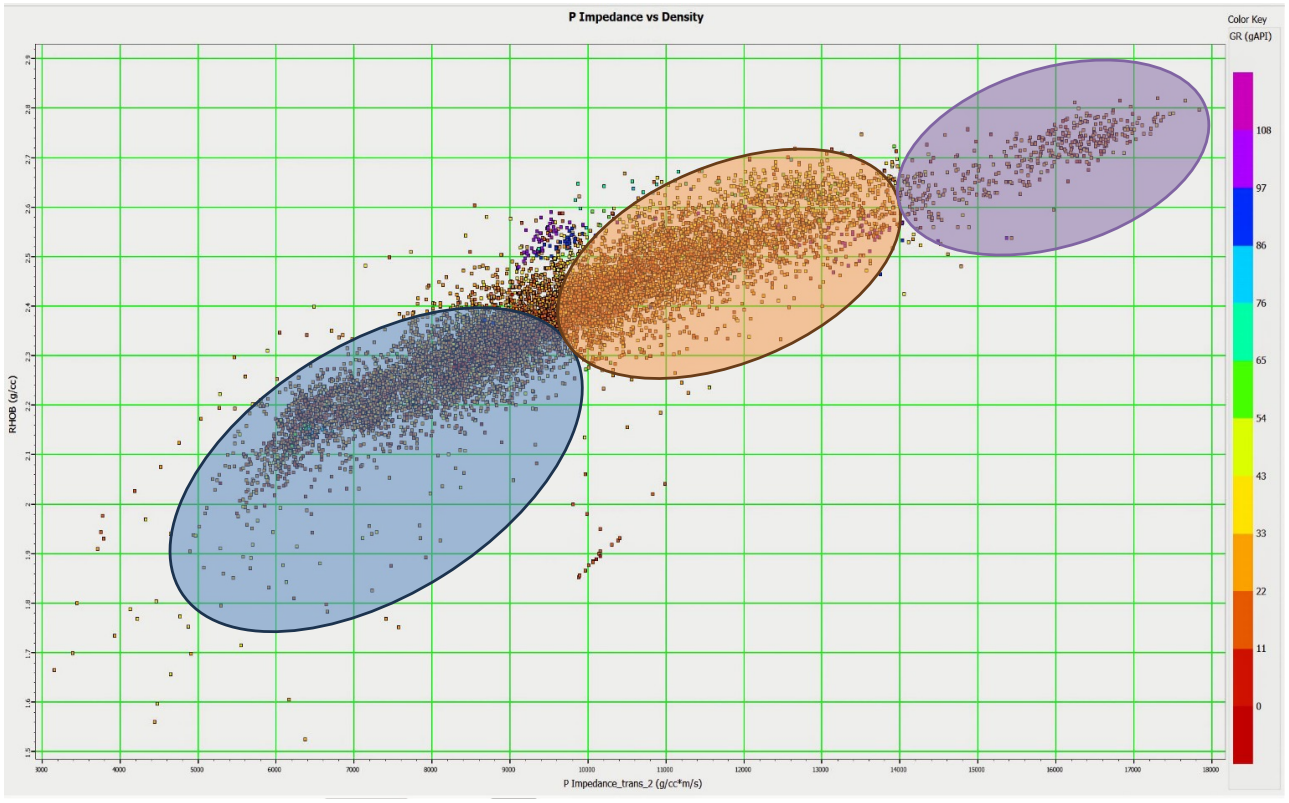

Figure 6. Cross-plot of P-impedance and density with color bar of gamma ray values in the GAAN-2 wells

Sensitivity analysis was not conducted for Wells GAAX-1 and GANG-4 due to insufficient data, that prevented meaningful evaluation through cross-plots.

Depth structure map

The depth structure map of the Terumbu Formation (Figure 7) illustrates the subsurface morphology of the study area, characterized by relatively shallow structural zones predominantly distributed in the western to central part (approximately 240000 320000), as indicated by yellow to green colors. Depth increases gradually toward the eastern part of the area, as indicated by cyan to blue shading, reflecting a regional eastward to southeastward structural dip. A prominent structural high is developed in the central area, coinciding by the location of several wells. Favorable conditions for carbonate reef development are provided by this positive relief, in alignment by the regional setting of the East Natuna Basin, where Miocene carbonate systems are known to have preferentially formed above localized basement-controlled highs (Darman 2017). The relatively tight contour spacing around this high suggests fault-related deformation that may influence structural closure and trap geometry. Hydrocarbon migration into the Terumbu carbonate reservoir may be facilitated by such fault systems; however, trap integrity could also be affected by structural reactivation, necessitating further validation through well data and seismic attribute analysis. At a regional scale, the structural framework of the Terumbu Formation is strongly controlled by the Natuna Arch, that separates the East Natuna Basin by the West Natuna Basin and exerts a major influence on carbonate development (Darman 2017).

A more complex structural configuration is depicted by the depth structure map of the Arang Formation (Figure 8), by shallower zones primarily observed in the central to western part of the study area (yellow green), while deeper areas are shown to extend toward the eastern margin (blue to purple). This variation in depth is considered indicative of stronger structural control and differential subsidence inside of the Arang interval compared to the Terumbu Formation. A major structural high is observed in the central area, where several wells are situated, emphasizing its significance for petroleum system evaluation. The Arang Formation has been established as a reservoir in the East Natuna Basin, by hydrocarbon accumulations typically associated by fault-bounded highs and inverted structures (Darman 2017). Steep structural gradients around the wells, indicated by closely spaced contours, reflect strong fault control, predominantly related to normal faulting, that may facilitate vertical and lateral hydrocarbon migration. However, these faults may also increase the risk of leakage or remigration. At the regional scale, the basin architecture is characterized by a graben horst system developed on the eastern flank of the Natuna Arch, including the Komodo and Sokang Grabens, that are recognized as key domains for hydrocarbon prospectivity (Darman 2017). Elevated structural traps have been produced by subsequent tectonic reactivation and are still considered prospective, although the presence of dry wells in adjacent areas indicates that trap integrity and timing continue to represent critical uncertainties.

Model based inversion

The quality of the seismic inversion was evaluated through a well-to-seismic tie (WST) analysis using a zero-phase wavelet. The extracted wavelet shows a maximum correlation coefficient of 0.806, indicating a good match among the synthetic and real seismic traces. Further validation of the inversion outcomes was conducted by comparing inverted and log-derived acoustic impedance, yielding a very high correlation coefficient of 0.993 and a low error value of 0.11. These outcomes indicate that the inversion model reliably represents subsurface elastic properties and is suitable for reservoir characterization purposes.

P-Impedance

The model-based P-impedance inversion along Line 02 near the GADO-3 well in the East Natuna Basin (Figure 9) reveals lateral variations in rock physical properties that reflect lithological changes and compaction effects inside of the target interval. Acoustic impedance (Zp) is controlled by both P-wave velocity and bulk density, making it

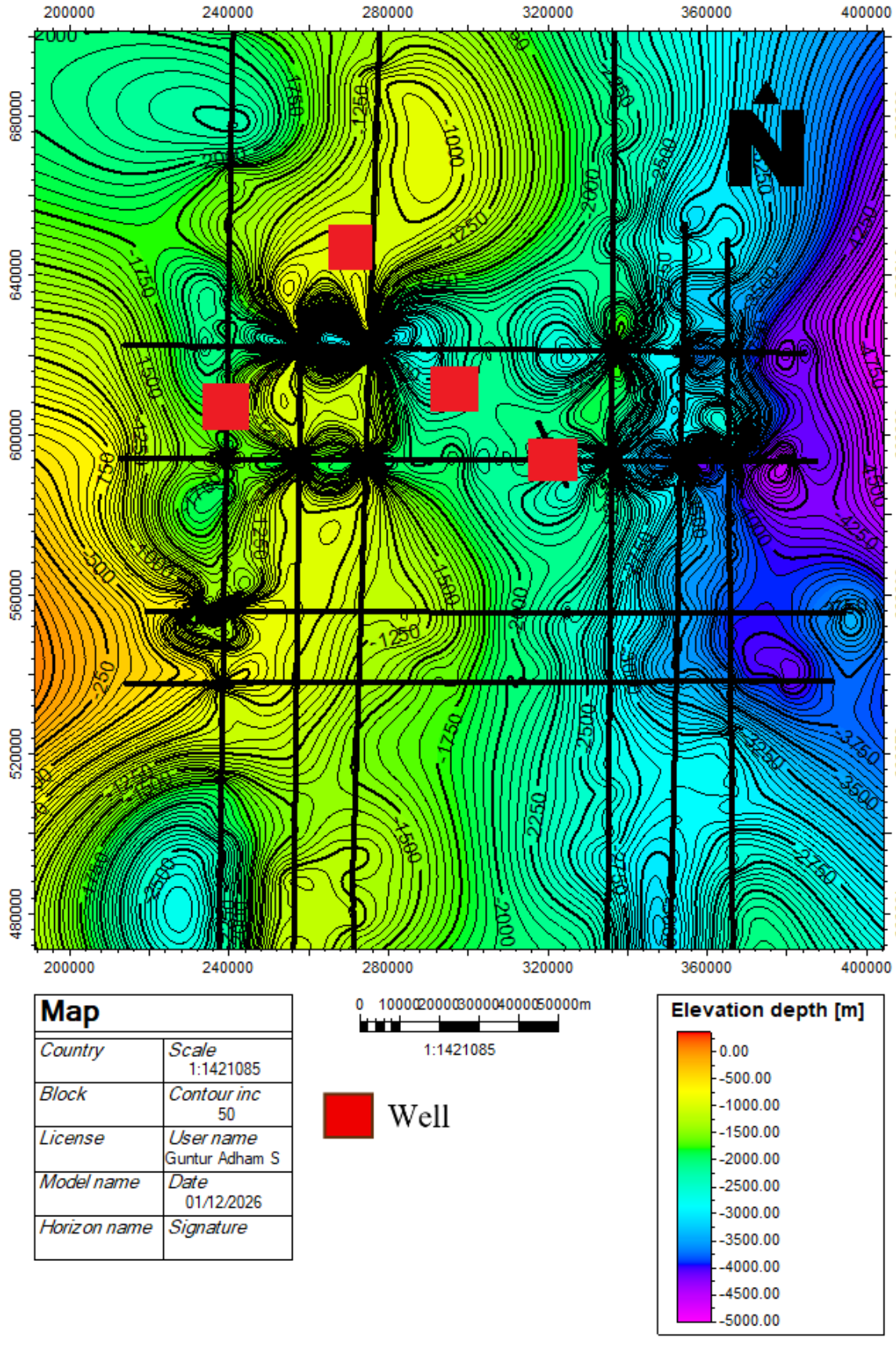

Figure 7. Depth structure map of the Terumbu formation in the East Natuna Basin.

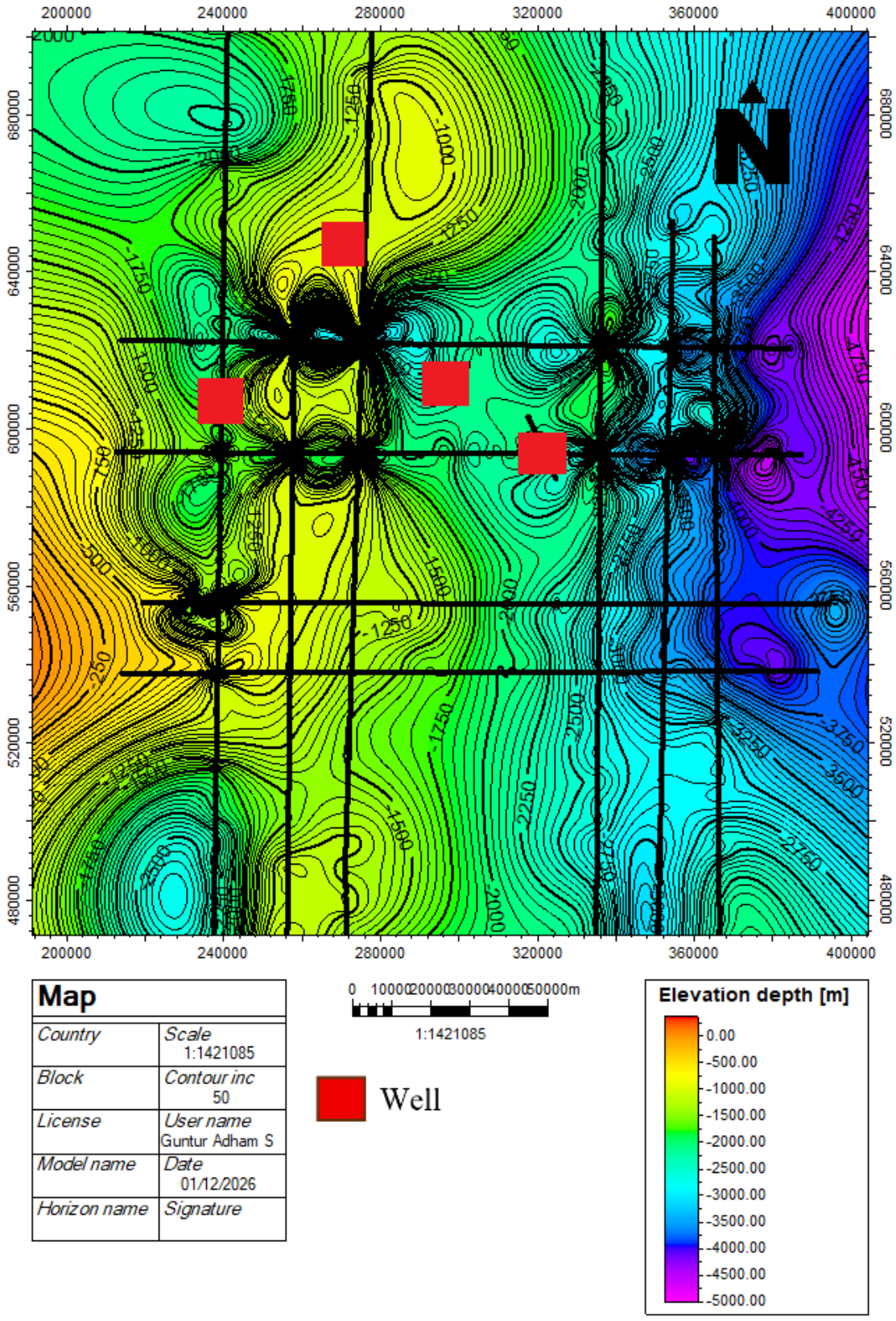

Figure 8. Depth structure map of the Arang formation in the East Natuna Basin.

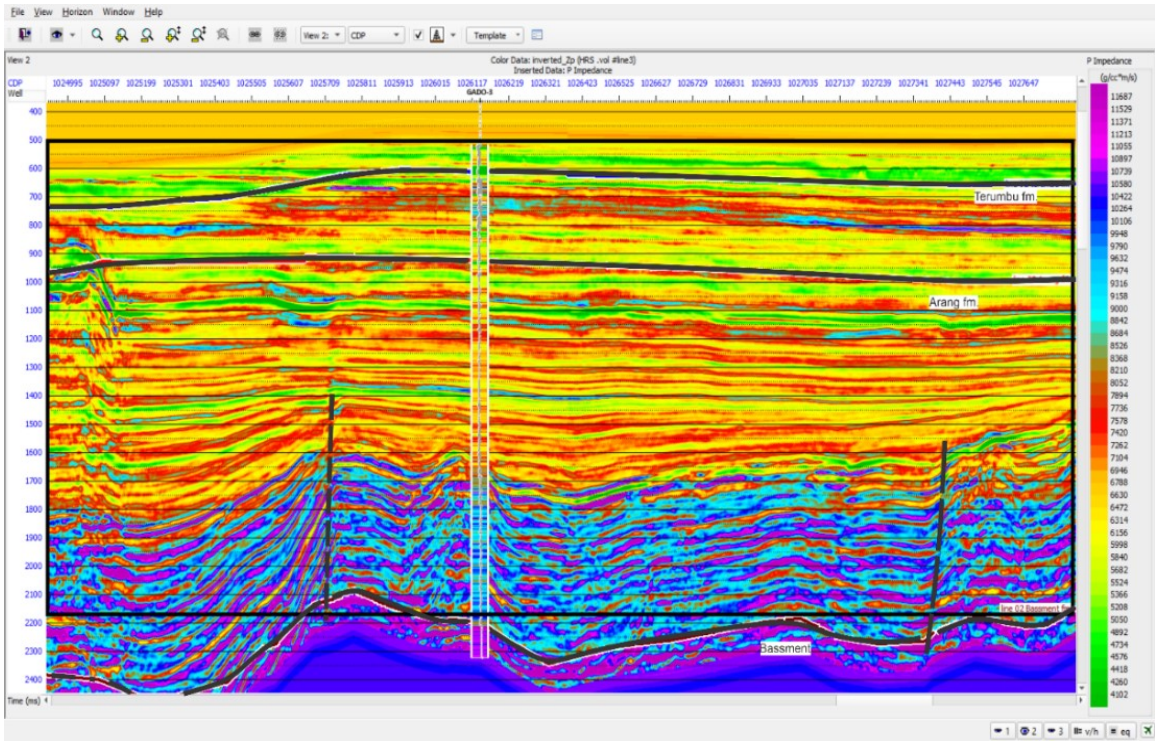

Figure 9. Model-based P-impedance inversion result on Line 02 near the GADO-3 well, East Natuna Basin. The figure illustrates the lateral acoustic impedance distribution within the target interval of the Terumbu and Arang Formations. The area of interest is highlighted by a black box to evaluate potential reservoir zones.

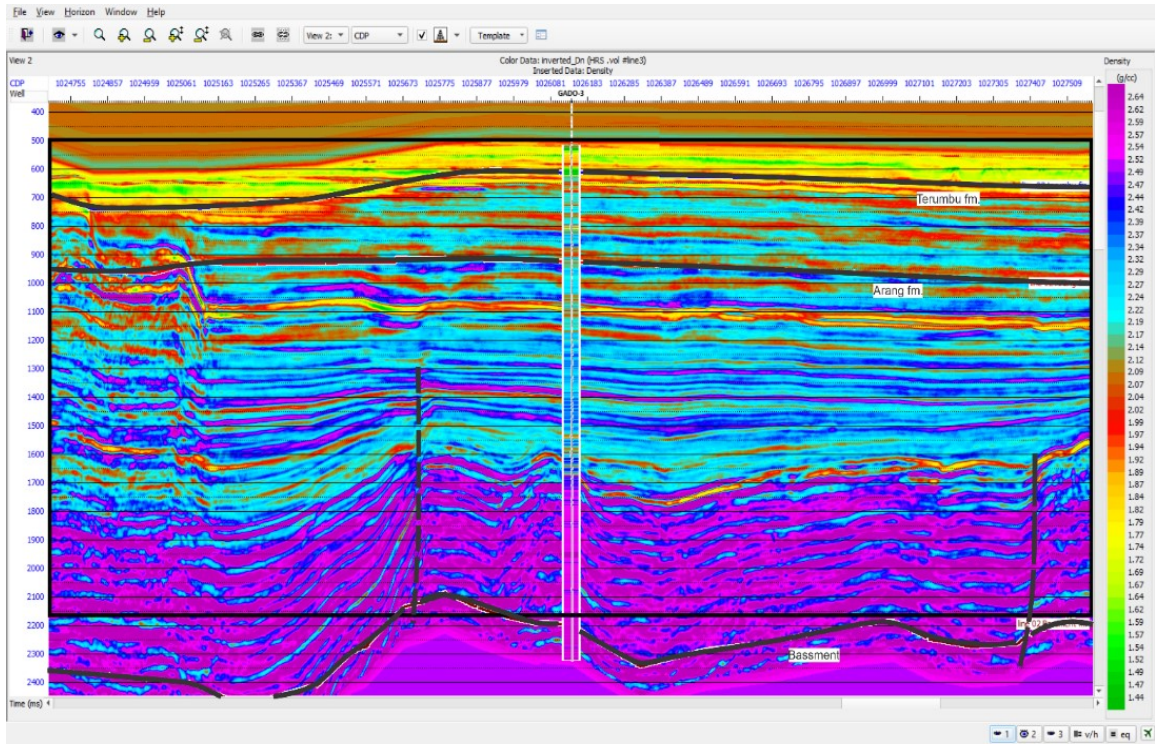

Figure 10. Density inversion model result on Line 02 near the GADO-3 well, East Natuna Basin. Increasing density values with depth support lithology differentiation between carbonate and clastic intervals within the Terumbu and Arang Formations. The black boxed area represents the main interpretation window.

particularly effective for discriminating stiff carbonate rocks by less compacted clastic units (Mavko et al., 2009; Dvorkin et al., 2014). Line 02 and Well GADO-3 were selected for this analysis because GADO-3 is the only well that fully penetrates the target reservoir interval, including the Reef and Arang formations, whereas the other three wells do not intersect these units.

Additionally, GADO-3 provides the most complete and reliable log dataset necessary for seismic inversion calibration, and Line 02 directly intersects this well, ensuring consistent well-to-seismic integration and improved interpretation quality. Low to moderate impedance values are observed (approximately 4,100 6,156 g/cc·m/s; green to yellow), indicating porous carbonate zones potentially affected by dissolution or fracturing that enhance secondary porosity (Anselmetti & Eberli, 2003). Toward 700 900 ms, the impedance increases to moderate high values (±6472 7894 g/cc·m/s; yellow red), suggesting increasing cementation and rock stiffness associated by burial-related diagenesis. Inside of the area of interest (black box), the Terumbu Formation exhibits heterogeneous impedance responses consistent by variability in carbonate facies. At the 500 700 ms interval, This behavior aligns by typical reef build-ups in Natuna, where the best porosity is generally found along the upper structural highs and progressively decreases downward (Wilson, 2011). Below the carbonate interval, the Arang Formation displays moderate to moderately high impedance values (±6472 7894 g/cc·m/s; yellow red) among 900 1600 ms, corresponding to compacted sandy shale lithology. Interbedded zones by lower impedance (±4102 5366 g/cc·m/s; green light green) suggest localized fine-grained sandstone streaks that may act as secondary reservoir pockets. At deeper intervals (1600 2200 ms), very high impedance is recorded (9000 11529 g/cc·m/s; cyan purple), indicative of highly compacted shale by diminished reservoir potential.

This trend reflects increasing burial stress and lithification associated by basinward compaction processes (Kessler et al., 2016). Overall, the impedance distribution confirms stiff and non-reservoir carbonate at the lower Terumbu interval and highly compacted shale in deeper sections of

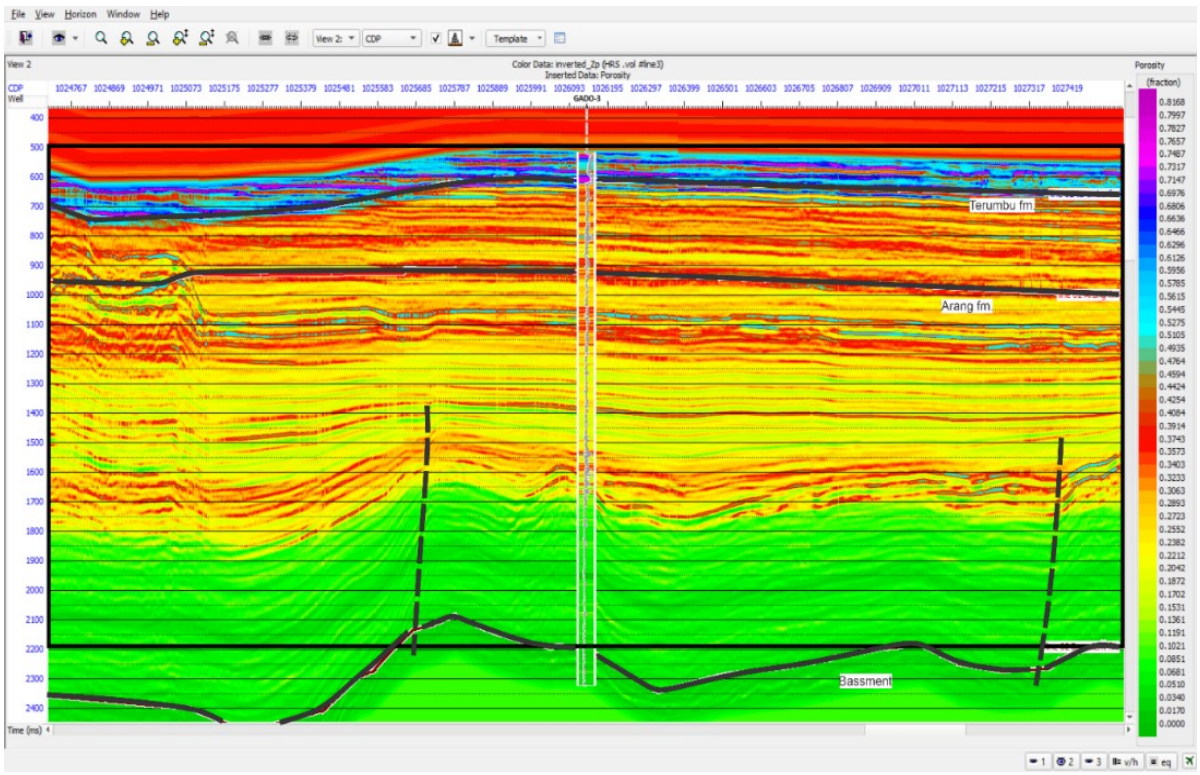

Figure 11. Porosity inversion model on Line 02 near the GADO-3 well, East Natuna Basin. The figure displays the reservoir quality distribution in the Terumbu and Arang Formations. The black box highlights zones with porosity anomalies interpreted as potential hydrocarbon-bearing intervals.

the Arang Formation, while the moderate to low impedance anomalies inside of the upper structural zone highlight the most prospective clastic and carbonate reservoir intervals.

Density

The density inversion model along Line 02 near the GADO-3 well (Figure 10) provides critical insights into lithological composition and compaction trends across the reservoir target in the East Natuna Basin The higher-density pockets likely represent tight carbonate zones or possible non-carbonate material infill that may degrade reservoir properties.

In the Terumbu Formation, carbonate units among 500 750 ms show relatively low to-moderate densities (1.57 1.77 g/cc; (green yellow)) by localized increases up to ~2.00 g/cc.

Lower density reflects porous limestone by limited diagenetic cementation, typical of early-stage reef development (Anselmetti & Eberli, 1993; Lucia 2007).

The higher-density pockets likely represent tight carbonate zones or possible non-carbonate material infill that may degrade reservoir properties.

In the lower Terumbu interval (750 900 ms), density increases (2.00 2.27 g/cc; red to cyan), by streaks reaching approximately 2.44 g/cc (blue), suggesting increased cementation and compaction that may act as an internal barrier or sealing zone — a possible transition toward the overlying clastic Arang Formation.

The Arang Formation, composed Predominantly composed of shaly sand and shale, this interval exhibits overall higher density influenced by compaction. The 900 1600 ms interval is observed to exhibit densities ranging by 2.22 to 2.44 g/cc (cyan blue), by sporadic occurrences of very high densities up to approximately 2.64 g/cc (purple), indicating the presence of shale-rich, compacted sequences (Lindseth, 1979). Below 1600 2200 ms, density increases further (2.59 2.70 g/cc; light to dark purple), reflecting intensified burial diagenesis and poor reservoir potential. These intervals may approach the transition into highly compacted sediments or basement rocks.

The overall stratigraphic trend demonstrates that density increases by depth while porosity diminishes, in accordance by the compaction-controlled diagenetic pathways of both carbonate and clastic systems (Anselmetti et al., 2003).

Porosity

The porosity inversion model along Line 02 near the GADO-3 well (Figure 11) illustrates the spatial variation of reservoir quality inside of the Terumbu and Arang formations. In the upper Terumbu Formation (500 700 ms), high porosity values ranging by 0.37 0.52 by localized anomalies up to 0.70 (red cyan purple)) -indicate well-developed porous carbonate lithofacies, likely corresponding to reef core or grain-supported facies by preserved primary porosity (Lucia 2007).

At 700 900 ms, porosity is observed to decrease to moderate levels (0.25 0.40; yellow red), consistent by flank or transition facies, where burial compaction and cementation progressively reduce pore connectivity. Despite this reduction, reservoir quality is still considered promising.

Inside of the Arang Formation, porosity is observed to become more variable due to clastic heterogeneity. The 900 1200 ms interval exhibits porosity values ranging by 0.22 to 0.35, by minor anomalies reaching approximately 0.50 (yellow red cyan), that are considered to correspond to isolated fine sandstone bodies encased inside of shale and potentially acting as stratigraphic hydrocarbon traps (Rider 1996).

Below 1200 1700 ms, porosity further declines to 0.13 0.21 by limited reservoir potential. The deepest interval (1700 2200 ms) shows very low porosity (<0.11; green shades), indicating highly compacted shale by reduced pore connectivity, consistent by increased burial stress and lithification (Mavko et al., 2009).

This continuous reduction in porosity is observed to correlate closely by the compaction and density increase recorded in both formations, reinforcing the interpretation that reservoir quality diminishes by increasing depth.

CONCLUSION

The characterization of the Terumbu and Arang formations in the East Natuna Basin has been significantly refined through integrated well-log interpretation, petrophysical sensitivity analysis, structural mapping, and model-based seismic inversion.

The Terumbu Formation is interpreted to represent a clean, porous carbonate reservoir, as indicated by low gamma ray values (18 24 API), high porosity (up to 0.28 in GADO-3 and 0.31 in GANG-4), and low clay content (0.06 0.15). Hydrocarbon presence is inferred by the neutron density crossover observed in GADO-3 (6808 6941 ft) and GANG-4 (2500 2569 ft), accompanied by elevated deep resistivity values (852 1997 Ù·m) in comparison to shallow resistivity (~3 Ù·m).

In contrast, the Arang Formation is observed to exhibit poor reservoir quality, as indicated by high gamma ray responses (102 148 API), clay volumes of 0.40 0.44, porosity values of 0.05 0.12, and resistivity of only 2 5 Ù·m, reflecting dominantly compacted shale by minimal sandstone development.

Cross-plot analysis confirms that acoustic impedance and bulk density effectively discriminate Terumbu carbonates by Arang shales. The Terumbu interval is observed to exhibit relatively low acoustic impedance (4,500 9,000 g/cc·m/s) and bulk density (1.70 2.35 g/cc), whereas significantly higher values are recorded in the Arang Formation (9,000 17,500 g/cc·m/s and 2.45 2.80 g/cc). Depth structure mapping reveals a central northern structural high (grid zone: 250,000 330,000), that is considered an optimal setting for reefal carbonate development and hydrocarbon entrapment.

Model-based seismic inversion serves as the primary tool for enhancing the detection of lithology and reservoir distribution. The upper Terumbu interval at 500 700 ms is characterized by low acoustic impedance (4100 6156 g/cc·m/s), low density (1.57 1.77 g/cc), and high porosity (0.37 0.52), confirming the presence of a high-quality carbonate reservoir. Impedance and density gradually increase by the lower Terumbu to the upper Arang intervals (6472 7894 g/cc·m/s and 2.22 2.44 g/cc) and reach maximum values inside of the lower Arang Formation (>9000 11529 g/cc·m/s and 2.59 2.70 g/cc), where porosity is reduced to <0.11, reflecting a tight, non-reservoir lithology.

Overall, the upper Terumbu Formation surrounding the structural high is considered the most prospective hydrocarbon target, particularly in the vicinity of Wells GADO-3 and GANG-4, where integrated geophysical and petrophysical indicators consistently demonstrate the presence of porous carbonate development and potential gas saturation. Additional well control and further seismic attribute calibration are recommended to improve the validation of hydrocarbon accumulation, reservoir connectivity, and volumetric assessment.

ACKNOWLEDGEMENT

The authors express their gratitude to the Center for Oil and Gas LEMIGAS for granting permission to utilize and publish the seismic and well data used in this study. Appreciation is also extended to Universitas Indonesia for providing academic support and research facilities throughout the completion of this work.

GLOSSARY OF TERMS & SYMBOLS

Terms & Symbol	Definition	Unit
AI	Acoustic Impedance	g/cc*m/s
Zp	P-wave Impedance	g/cc*m/s
Vp	P-wave Velocity	m/s
RHOB	Bulk Density	g/cc
NPHI	Neutron Porosity	fraction
GR	Gamma Ray	API
RESD	Deep Resistivity	Ω·m
RESM	Medium Resistivity	Ω·m
MSFL / LLS	Micro Spherically Focused Log / Laterolog Shallow	Ω·m
LLM	Laterolog Medium	Ω·m

LLD	Laterolog Deep	Ω·m
Sw	Water Saturation	fraction
TWT	Two-Way Time	ms
PSTM	Post Stack Time Migration	—
Zoeppritz Eq.	Zoeppritz Equation	—
Rho	Density	g/cc
AI Model	Model-Based Acoustic Impedance	g/cc*m/s

REFERENCES

Anselmetti et al., (1993), Control on Sonic Velocity in Carbonates, PAGEOPH Vol. 141 No 2/3/4, Birkhauser Verlag, Basel.

Anselmetti et al., (1997), Acoustic properties of Neogene carbonates and siliciclastics from the subsurface of the Florida Keys: implications for seismic reflectivity, Marine Geology 144 9-13, Elsevier Science B.V.

Anselmetti et al., (2003), Factor controlling elastic properties in carbonates sediments and rock, The Leading Edge, SEG, United States.

Ashraf. U. et al., (2022), Estimation of porosity and facies distribution through seismic inversion in an unconventional tight sandstone reservoir of Hangjinqi area, Ordos basin, Front. Earth Sci. 10:1014052. doi: 10.3389/feart.2022.1014052.

Asquith & Krygowski, (2004), Basic Well Log Analysis, The American Association of Petroleum Geologist, Oklahoma.

Assefa S. et al., (2003), Velocities of compressional and shear waves in limestone, Geophysical Prospecting 51, 1-13, European Association of Geoscientists Engineers.

Bashir Y. et al., (2021), Seismic expression of miocene carbonate platform and reservoir characterization through geophysical approach: application in central Luconia, offshore Malaysia, Journal of Petroleum Exploration and Production Technology (2021) 11:1533–1544.

Bashir Y. et al., (2024), Cohesive approach for determining porosity and P-impedance in carbonate rocks using seismic attributes and inversion analysis, Journal of Petroleum Exploration and Production Technology (2024) 14:1173–1187.

Cakra. Y.I., (2021), Evaluating Oligocene Intra Platform Reef Carbonate Reservoir Potential Using Advance Model of Seismic Facies Analysis and Seismic Inversion A Case Study Barito Basin Indonesia, Proceedings Joint Convention Bandung (JCB) 2021.

Chopra & Marfut (2007), Seismic Attributes for Prospect Identification and Reservoir Characterization, Society Of Exploration Geophysicits, Oklahoma.

Darman. H, (2017), Seismic Expression Of Key Geological Features In The East Natuna Basin, Berita Sedimentologi, Indonesia.

Durrani. M.Z.A et al., (2021), Characterization of carbonate reservoir using post-stack global geostatistical acoustic inversion approach: A case study from a mature gas field, onshore Pakistan, Journal of Applied Geophysics 188 (2021) 104313.

Dewan. J.T., (1983), Essential of Modern Open-Hole log Interpretation, PennWell Publishing Company, Oklahoma.

Dvorkin, J., et al., (2014), Seismic Reflections of Rock Properties. Cambridge Univ. Press. United States.

Ellis. D & Singer. J., (2007), Well Logging for Earth Scientists, Springer, Dordrecht Netherlands.

El-Sayed. A.S. et al., (2024), Utilizing post-stack seismic inversion for delineation of gas bearing sand in a pleistocene reservoir, baltim gas field, nile delta, Egypt, scientific reports, natureportofolio.

Espejel. R.L., et al, (2019), Distribution and growth styles of isolated carbonate platforms as a function of fault propagation, Marine and Petroleum Geology Volume 107, September 2019, Pages 484-507, Elsevier.

Falade. A.O. et al., (2024), Hydrocarbon prospective study using seismic inversion and rock physics in an offshore field, Niger Delta, Research Discover Geoscience, Discover.

Handoyo. H., Ronlei Bernard Cavin, Wibowo Andy Setyo, Sigalingging Asido Saputra, Nathania Edlyn Yoadan, Fatkhan. F., Erdi Aurio, Avseth Per, Carbonell Ramon, Nugroho Pranowo, Pandito Riky Hendrawan Bayu, Nasibov Aladin, Husein Abdullah Ali, (2025), Reservoir Characterization of Ngrayong Formation, Sandstone with Carbonate Intercalation, Using a Geostatistical Approach Based on Petrophysical Parameters, Northeast Java Basin, Indonesia, Scientific Contributions Oil & Gas, Vol. 48. No. 3, LEMIGAS, Jakarta. https://doi.org/10.29017/scog.v48i3.1828.

Handoyo. H., Ronlei , 2024, Characterization of Carbonate Reservoir Potential in Salawati Basin, West Papua: Analysis of Seismic Direct Hydrocarbon Indicator (DHI), Seismic Attributes, and Seismic Spectrum Decomposition, Indonesian Journal on Geoscience Vol. 11 No. 2 August 2024: 173-188.

Hendry. J. et al., 2021, Seismic Characterization of Carbonate Platforms and Reservoirs, Geological Society London Special Publications, 509,1–28, The Geological Society of London.

Hutchison. C., 2014, Tectonic evolution of Southeast Asia, Bulletin of the Geological Society of Malaysia, Volume 60 pp. 1-18, Malaysia.

Jammaludin & Battu Desianto Payung 2026, Characterization Of Deltaic Source Rocks And Hydrocarbon Potential In The Lower Kutai Basin, Scientific Contributions Oil & Gas, Vol. 49. No. 1, LEMIGAS, Jakarta.

Janjuhah. H.T. et al., 2021, Integrated Porosity Classification and Quantification Scheme for Enhanced Carbonate Reservoir Quality: Implications from the Miocene Malaysian Carbonates, Journal of Marine Science and Engineering, 9,1410, MDPI, Switzerland.

Johnson. A.B. & Cullen A.B., 2023, Continental rifting in the South China Sea through extension and high heat flow: An extended history, Gondwana Research 120 (2023) 235-263, Elsevier.

Kessler F. & Jong. J., 2016, The South China Sea: Sub-basins, Regional Unconformities and Uplift of the Peripheral Mountain Ranges since the Eocene, Berita Sedimentologi, Indonesia.

Koesoemadinata, R.P., 1980, Geologi Minyak dan Gas Bumi, Jilid 1, Institut Teknologi Bandung, Bandung.

Kuszpit W.K & Sowizdzal K., 2024, Integration of Well Logging and Seismic Data for the Prognosis of Reservoir Properties of Carbonates, Energies 2024, 17, 355, MDPI, Switzerland.

Larki E. et al., 2023, A new insight to access carbonate reservoir quality using quality factor and velocity deviation log, Acta Geophysica (2024) 72:3159–3178.

Lauwijaya W.S. et al., 2024, Integrated Reservoir Characterization in a Newly Discovered Area of the South Mahakam Cluster: Navigating Challenges and Opportunities, PIT IAGI Balikpapan 2024.

Lindseth, R.O., 1979, Synthetic sonic logs-a process for stratigraphic interpretation, Geophysics Vol. 44 No 1 P. 3-26, 22 Figs, Society Of Exploration Geophysicits, Oklahoma.

Lucia. F., 2007, Carbonate Reservoir Characterization, Springer, Dordrecht Netherlands.

Mathew M., et al., 2020, The Emergence Of Miocene Reefs In South China Sea And Its Resilient Adaptability Under Varying Eustatic, Climatic And Oceanographic Conditions, Scientific Reports, natureresearch.

Mavko, G., Mukerji, T., & Dvorkin, J. ,2009, The Rock Physics Handbook, Cambridge Univ. Press. United States.

Mirshadi A. et al., 2024, Estimation of pore-type distribution utilizing petrophysical data and rock physics modeling on an Iranian carbonate reservoir, Journal of Petroleum Exploration and Production Technology (2024) 14:2379–2397. Springer.

Naseer M.T., et al., 2024, Seismic attributes and spectral decomposition-based inverted porosity-constrained simulations for appraisal of shallow -marine lower-Cretaceous sequences of Miano gas field, Southern Pakistan, Heliyon 10 (2024) e25907, Elsevier.

Pangastuti. Ni Putu Juliyant Ananda Rika, Rosid Mohammad Syamsu, Wijanarko Edy, 2025,

Binio Formation Characterisation Using Seismic Acoustic Impedance Inversion in the Lotus Field of the Central Sumatra Basin, Scientific Contributions Oil & Gas, Vol. 48. No. 2, LEMIGAS, Jakarta. https:// doi.org/10.29017/scog.v48i2.1692 .

Pramudito D., et al., 2021, Enhancing Low-Frequency Model for Post-Stack Inversion using Geostatistics: A Case Study in Imaging Carbonate Structure, Jurnal Geofisika (2021) Vol. 19, No. 02 pp. 69-73, HAGI.

Rider, M., 1996, The Geological Interpretation of Well Logs, Rider-French Consulting Ltd, Scotland.

Rose et all., 2025, Telisa Formation Characterization Using Seismic Acoustic Impedance Inversion In The Akasia Area of The Central Sumatra Basin, Scientific Contributions Oil & Gas, Vol. 48. No. 2, August: 29 – 40, LEMIGAS, Jakarta

Russell. B., 1988, Introduction to Seismic Inversion Methods, Society Of Exploration Geophysicits, Oklahoma.

Salvini S., et al., 2023, Exploring the pore system of carbonate rocks through a multi-analytical approach, Environmental Earth Sciences (2023) 82:564, Springer.

Schlumberger, 2016, Basic Well Log Interpretation. The Defining Series:.

Serra. O., 2003, Well Logging and Reservoir Evaluation, Technip, Paris.

Sheriff. R. & Geldart. L., 1995, Exploration Seismology, Cambridge Univ. Press. United States.

Su. Zhaodong., et al., 2023, Seismic prediction of porosity in tight reservoirs based on transformer, Frontiers in Earth Science. Frontiers.

Taqiy. Zalfadhiyaa Fariz., Utomo. Warto, Shidqii Muhammad, Susilo Adi, 2025, Karakterisasi Reservoar Berdasarkan Analisis Inversi Seismik Impedansi Akustik dan Multiatribut Seismik, Studi Kasus: Lapangan Bunyu Tapa, Cekungan Tarakan, Kalimantan Utara, Lembaran Publikasi Minyak dan Gas Bumi Vol. 59 No 3, LEMIGAS, Jakarta. https://doi.org/10.29017/ LPMGB.59.3.1891.

Wadas S.H. & Hartmann H. V., 2022, Porosity estimation of a geothermal carbonate reservoir in the German Molasse Basin based on seismic amplitude inversion, Geothermal Energy 10:13.

Wang. Zi-Zhen., et al., 2021, Empirical rock physics relationships on carbonate dry-frame elastic properties, Petroleum Science (2021) 18:783–806, Springer.

Weger. R. et all., 2009, Quantification of pore structure and its effect on sonic velocity and permeability in carbonates, AAPG Bulletin, v. 93, no. 10, The American Association of Petroleum Geologist, Oklahoma.

Wibowo. Rahmat Catur., et al., 2023, Analysis of Unconventional Oil and Gas Reservoirs using Well Logging, Geochemical and Seismic Data, Jurnal Geocelebes Vol. 7 No. 2. Departement of Geophysics Hasanuddin University. Makasar.

Wilson. M.E.J., 2011, SEAsian carbonates: tools for evaluating environmental and climatic change in equatorial tropics over the last 50 million years, Geological Society London Special Publications 2011, p344-372, The Geological Society of London, London.

Xu. Guoqiang & Haq B.U., et al., 2022, Seismic facies analysis: Past, present and future, Earth-Science Reviews Volume 224, January 2022, 103876. Elsevier.

Yang. Zhen., et al., 2024, Types and Evolution of the Miocene Reefs Based on Seismic Data in the Beikang Basin, South China Sea, Journal of Marine and Engineering 12,360, MDPI, Switzerland.

Zulivandama, S.R., Hermansyah, G.M. & Wijaksono, E., 2018, Aplikasi Metode Sweetness dan Spectral Decomposition untuk Identifikasi Awal Potensi Hidrokarbon di Perairan Utara Bali. Jurnal Geologi Kelautan.